

Complex Surface Structure of (110) Terminated Strontium Titanate Nanododecahedra

Lawrence A Crosby^a Robert M Kennedy^b Bor-Rong Chen^a Jianguo Wen^c
Kenneth R Poeppelmeier^b Michael J Bedzyk^a Laurence D Marks^{a*}

^a Department of Materials Science and Engineering, Northwestern University, Evanston, IL 60208

^b Department of Chemistry, Northwestern University, Evanston, IL 60208

^c Center for Nanoscale Materials, Argonne National Laboratory, Lemont, IL 60439

* Corresponding author.

Supporting Information

X-ray Analysis

XRD data of the STO dodecahedra, a $\theta - 2\theta$ scan from 20° to 80° is shown in Figure S1, in which the Bragg peaks were indexed with MDI Jade software. From the XRD profile, all the major diffraction features of the powder sample can be identified as cubic SrTiO_3 with negligible impurities. The positions and the relative intensities in between the peaks are consistent with SrTiO_3 with a lattice constant of 3.903 \AA .

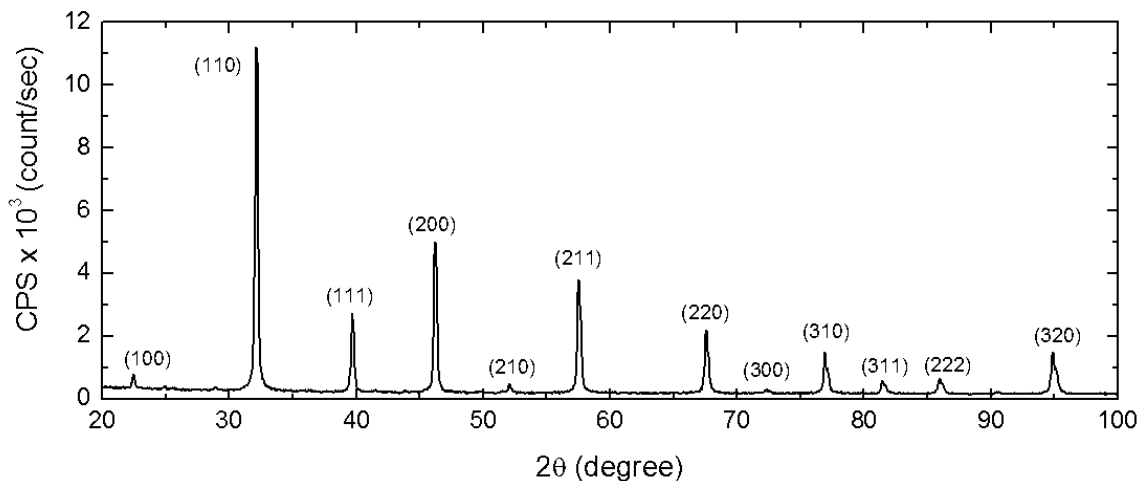


Figure S1: XRD data for the STO nanododecahedra

The Scherrer equation (eq. S1) is used to analyze the crystalline domain size of the STO nanoparticles:

$$L_{hkl} = \frac{0.9\lambda}{\beta \cos \theta} \quad (\text{S1})$$

where L is the crystalline size in the $[hkl]$ direction, 0.9 is the Scherrer constant, λ is the incident X-ray wavelength (1.542 Å for Cu K α source), θ is the angular peak position, and β is the integral breadth. Figure S2a shows the (110) diffraction peak of the nanododecahedra. The peak shape was fitted using a Lorentzian function given by

$$f(x) = A \frac{w/2}{(x - x_0)^2 + (w/2)^2} + Bx + y_0 \quad (\text{S2})$$

where A is the scaling factor, B and y_0 are fitting constants for the linear background, and the w and x_0 terms give the peak full width half maximum (FWHM) and the position, respectively. The integral breadth (β) for Lorentzian peak shape is related with the FWHM via:

$$\beta = \left(\frac{\pi}{2}\right) FWHM \quad (\text{S3})$$

The additional peak broadening by the instrument contribution was also taken into consideration in determining the peak broadening contributed by the crystallite size. 325 mesh single crystal Si powder was used as a standard to determine the instrumental peak width. The Si powder has a large crystallite size (44 μm), which minimized the peak broadening from size effects (Figure S2b). For Lorentzian peaks, the peak width due to the size of crystalline domains is obtained by subtracting the instrumental width from the measured peak width. The calculation led to an average crystalline domain size of 180 nm, which is consistent with that observed by TEM.

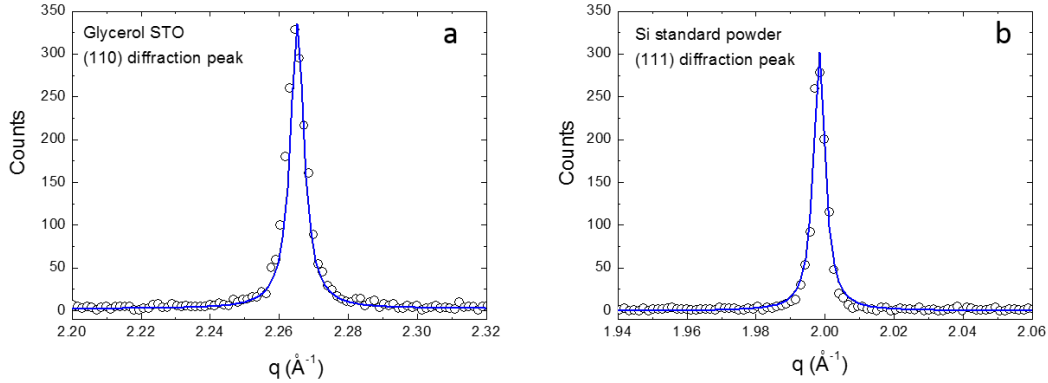


Figure S2: XRD peaks of a) (110) peak of STO dodecahedra and b) (111) peak of the 325 mesh Si powder. By applying the modified Scherrer equation (eq. S1), the mean crystallite size in the (hkl) can be determined from the broadening of the (hkl) diffraction peak.

XPS Analysis

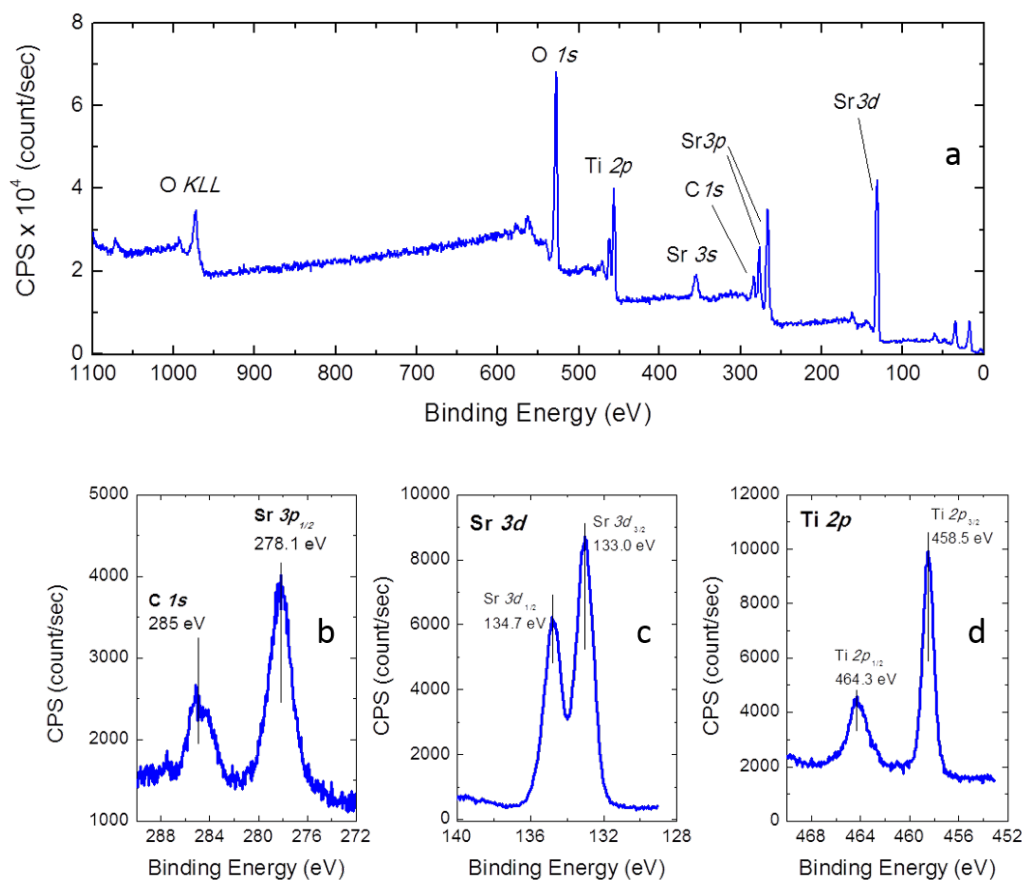


Figure S3: a) XPS Survey Spectrum as well as b) Sr 3p_{1/2} and C 1s peaks c) Sr 3d and d) Ti 2p peak positions.

The XPS survey spectrum in Figure S3 shows the core-level peaks of Sr, Ti and O elements and no evidence of contamination or strongly adsorbed hydrocarbons.

The peak positions are consistent with reference spectra for crystalline SrTiO₃ (see¹). The carbon 1s peak resulted from the air exposure of the sample and was calibrated to 285 eV.

EDS Analysis

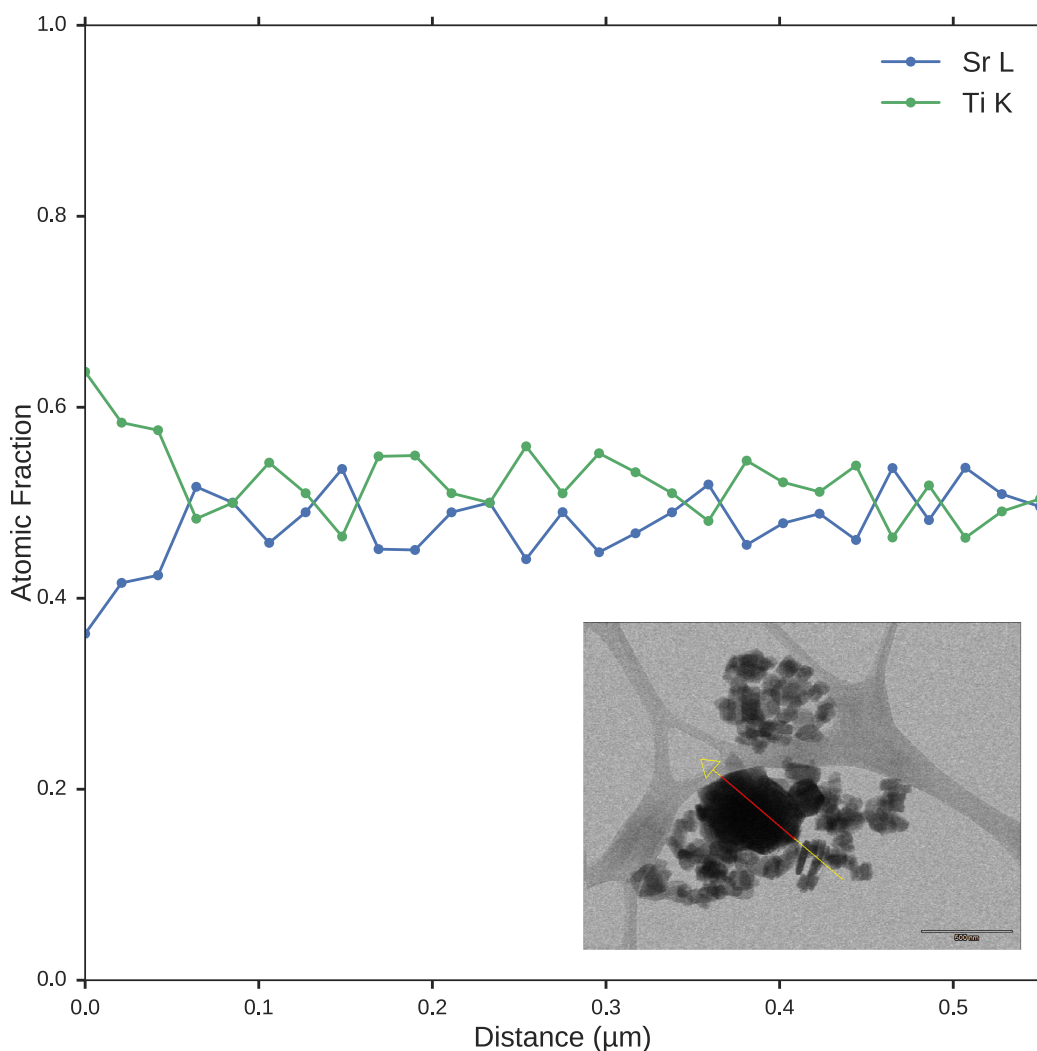


Figure S4: Plot of EDS linescan across nanoparticle with inset of a bright field image showing the location of linescan.

An EDS linescan (processed with the Cliff-Lorimer method) Figure S4 show that the Sr:Ti ratio is approximately 1:1.

HREM Quantitative Analysis

The first step was to obtain reasonable estimates for the microscope parameters such as accelerating voltage, spherical aberration, focal spread, and beam tilt. To do so, a map consisting of a montage of simulated motifs was constructed using the crystal structure of the known material and the aforementioned parameters for a range of thicknesses and defoci, then used to qualitatively match the experimental results for the bulk unit cells. The free parameter was crystal tilt, which was varied in steps of 2 mRad

and 5 degrees azimuthal rotation. Comparing several maps, the best qualitative results were chosen for further refinement using the normalized cross correlation coefficient (NCCC) statistic (see reference^{2,3}):

$$NCCC = \frac{\sum_x \sum_y (f(x, y) - \bar{f}_{u,v})(t(x - u, y - v) - \bar{t})}{\sqrt{\sum_x \sum_y (f(x, y) - \bar{f}_{u,v})^2 (t(x - u, y - v) - \bar{t})^2}} \quad (S4)$$

where $\bar{f}_{u,v} \equiv \frac{1}{N_x N_y} \sum_{x=u}^{u+N_x+1} \sum_{y=v}^{v+N_y+1} f(x, y)$

Here $f(x, y)$ represents the experimental image, t is the template or simulated image that is being compared directly with the experimental image, and (x, y, u, v) are the position and shifts in position of the template found relative to the experimental image. After maximizing the NCCC for the bulk simulated motifs, these results were then used to simulate several test surface structures without changing any of the conditions.

For particles imaged along the [001] zone axis, the thickness (see Figure S5a) follows the relationship $t = \frac{2\sqrt{3}}{3}x + t_0$ where x is the position relative to the edge and t_0 is the initial thickness. The corresponding form is $t = 2\sqrt{3}x + t_0$ for the [110] zone (see Figure S5b).

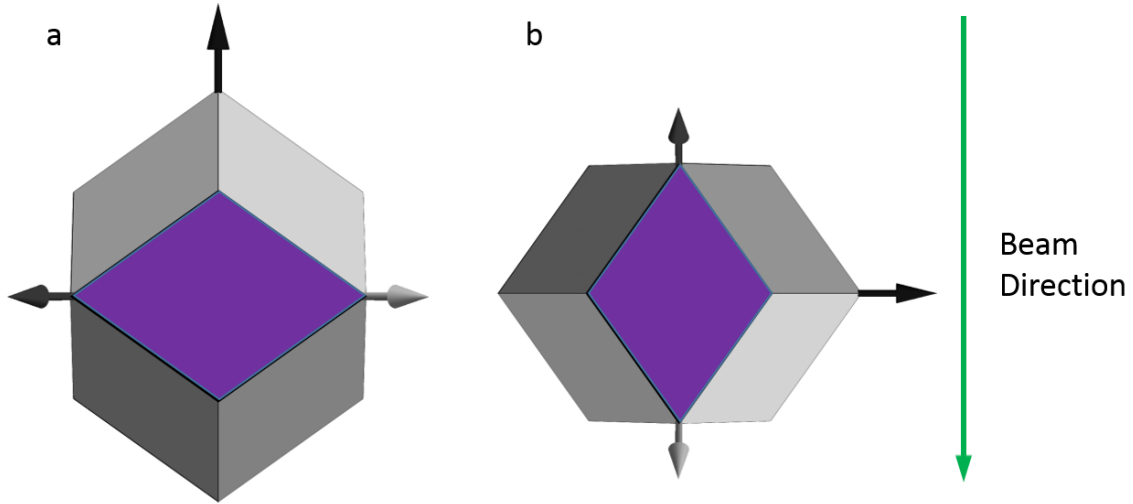


Figure S5: Geometry of (110) facet viewed edge on along a) [001] and b) [110] zone axes. The electron beam direction is parallel to the facet.

The imaging parameters were fitted as described in the methods section results, with the quantitative comparison using the NCCC appearing in Tables S1, S2. The defocus/thickness maps compared with wide area HREM experimental images for both the [001] and [110] zone axes (see Figure S6) show good qualitative agreement.

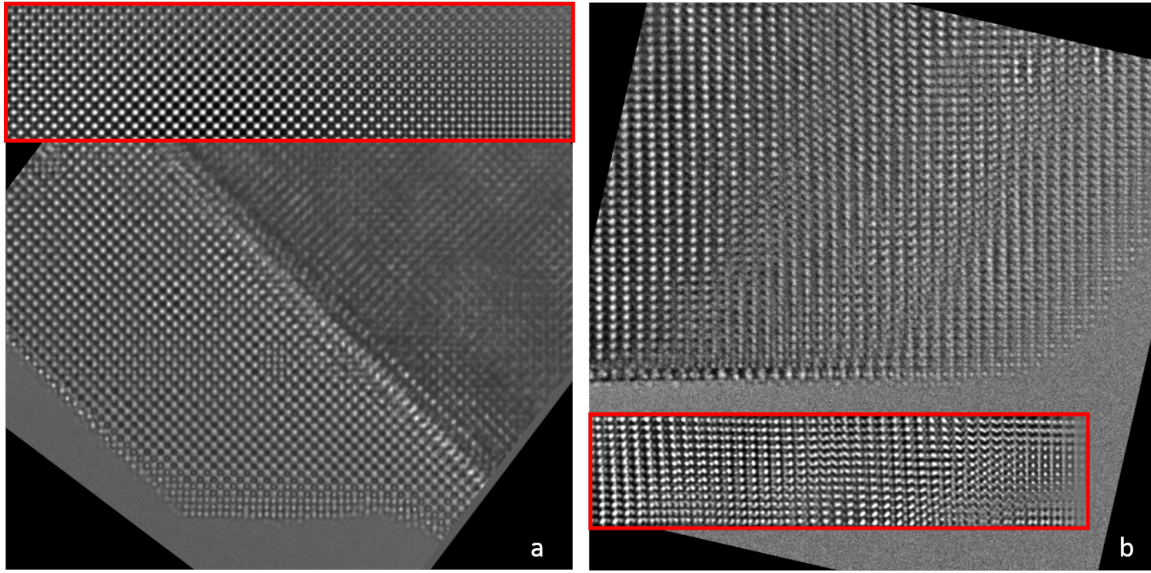


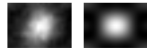
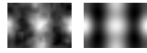
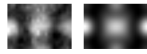
Figure S6: Defocus/Thickness map for sample viewed along the [001] zone axis a) and [110] zone axis b)

Table S1: NCCF for experimental (left) and simulated (right) bulk motifs imaged along the [001] zone axis. The imaging parameters for simulated images for this zone were $C_s=-0.005\text{mm}$, $C_s5=0\text{mm}$, $\alpha=0.5\text{ mrad}$, and $\Delta\text{df}=30\text{\AA}$.

Motif	Thickness (\AA)	Defocus (\AA)	NCCC
	82	90	0.984
	50	90	0.959
	50	70	0.930
	26	70	0.923

Table S2: NCCF for experimental (left) and simulated (right) bulk motifs imaged along the [110] zone axis. The imaging parameters for simulated images for this zone were $C_s=-0.015\text{mm}$, $C_s5=0\text{mm}$, $\alpha=0.5\text{ mrad}$, and $\Delta\text{df}=30\text{\AA}$.

Motif	Thickness (\AA)	Defocus (\AA)	NCCC
	72	-10	0.935

Motif	Thickness (\AA)	Defocus (\AA)	NCCC
	105	60	0.924
	11	90	0.896
	66	70	0.885

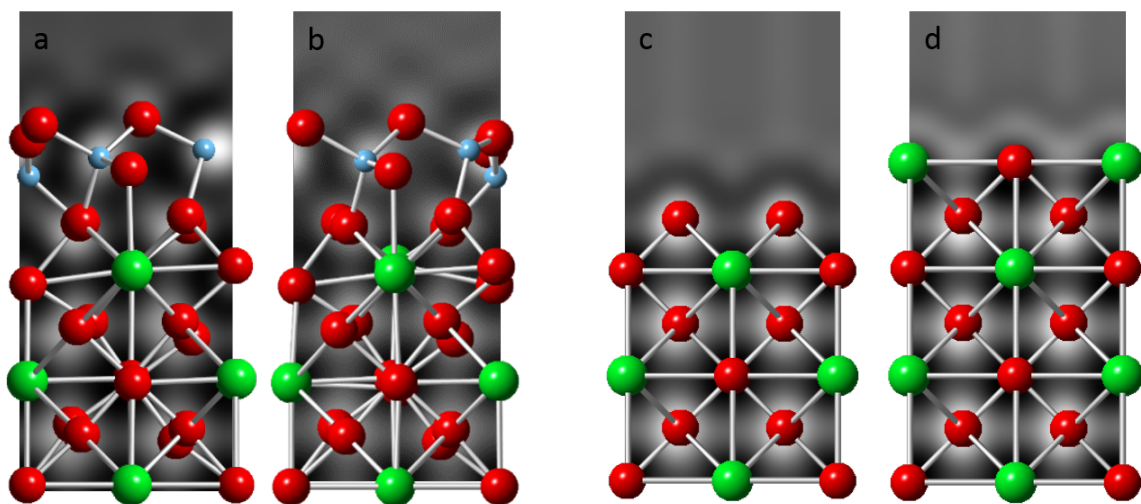


Figure S7: Atomic model overlaid with simulation with optimal parameters (defocus-50 \AA , thickness 58 \AA) for a) (3×1) and b) (4×1) c) O and d) SrTiO along [001] zone axis

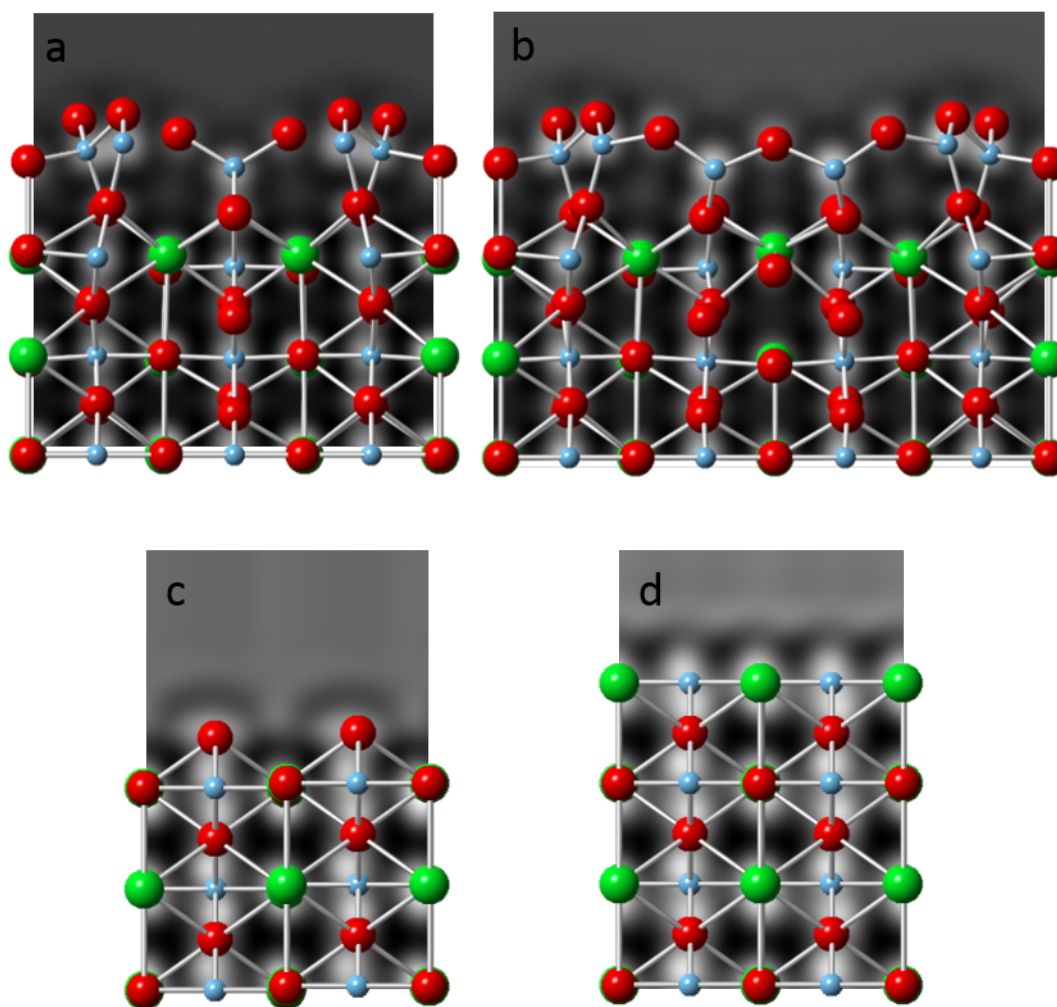


Figure S8: Atomic model overlaid with simulation with optimal parameters (defocus-60Å, thickness 6Å) for a) (3 × 1) and b) (4 × 1) c) O and d) SrTiO along $[1\bar{1}0]$ zone axis

References

- 1 R. P. Vasquez, *Surf. Sci. Spectra*, 1992–1992, **1**, 129–135.
- 2 K. Briechle and U. D. Hanebeck, in *Proc. SPIE*, 2001, vol. 4387, pp. 95–102.
- 3 J. P. Lewis, *Vis. Interface*, 1995, **10**, 120–123.